JOURNAL OF MATERIALS SCIENCE 23 (1988) 3073–3082

Fracture toughness and molecular structure of unfilled epoxy adhesives

JESSICA A. SCHROEDER
Polymers Department, General Motors Research Laboratories, Warren, MI 48090-9055, USA

The cohesive, mode I (tensile cleavage) fracture energy (or fracture toughness), G_{Ic}, of bulk tapered double cantilevered beam (TDCB) samples of a series of three epoxy thermoset networks was determined using a linear elastic fracture mechanics (LEFM) analysis. Networks of different crosslink density were obtained by mixing various amounts of an aromatic epoxy novolac and an aliphatic epoxy and crosslinking with an imidazole catalyst. Brittle, stick–slip fracture was observed for all formulations, with G_{Ic} increasing as the amount of aliphatic epoxy increased. However, fracture surface morphologies exhibited evidence of increasing plastic deformation as G_{Ic} increased. In the investigation of structure–property relationships for this series of thermoset networks, G_{Ic} was found to be inversely related to both network crosslink density and glass transition temperature (T_g). It was also found that the room temperature frequency of the glassy state transition (β-transition) increased as fracture toughness increased.

1. Introduction

The use of crosslinked epoxies as structural (load-bearing) engineering materials in automotive, aerospace, and marine industries is continually increasing. For example, motivated by the need to join dissimilar materials such as steel, galvanized steel, aluminium, and a variety of polymeric materials, a concerted effort has been made to replace mechanical joints (bolts and welds) by structural adhesive joints. In addition to the ability to bond dissimilar materials, the advantages of adhesive bonding include uniform stress distribution, higher strength-to-weight ratios, and less sensitivity to corrosion. However, effective use of structural adhesives requires a knowledge of their response to complex loading modes and adverse environmental conditions. Ultimately this means that the relationships between fracture processes and chemical and physical structure must be understood.

The fracture of structural adhesives in bonded joints is generally characterized by the propagation of cracks from existing flaws. These flaws, which act as stress concentrators, are introduced into the adhesive during processing in the form of air bubbles, dirt particles, oil contaminants, and/or non-bonded areas. Additionally, polymer damage, with associated flaws, may develop during service due to aggressive environmental conditions or fatigue loading. Thus, the design limitations of a joint will be governed in large part by the adhesive's ability to resist the propagation of cracks, i.e., by its toughness. Therefore, determining the fracture toughness of a given adhesive in various joint geometries and under various environmental conditions is a necessary part of evaluating the material for a specific adhesive application. Also, correlating the chemical and physical structure of adhesive materials with their fracture toughness will aid in the design of tough, durable adhesives.

Using a continuum mechanics energy balance approach, Griffith [1] postulated that for brittle, linear elastic materials, crack propagation occurs when the energy released from a stress field equals the energy required to create new surfaces. However, since actual fracture energies, except for the most brittle of materials, are orders of magnitude greater than the energies required to break covalent bonds, other energy absorbing processes must be involved. Orowan [2] and Irwin [3] modified Griffith's treatment by replacing the surface energy term with a critical strain energy release rate, G_c, which includes plastic and viscoelastic dissipation, as well as elastic (surface) energy terms. The surface energy is a small component of G_c. Thus, the linear elastic fracture mechanics (LEFM) analysis may be applied to materials which exhibit linear elastic stress–strain behaviour overall, but which undergo inelastic processes in the small region surrounding the crack tip. G_c is referred to as the fracture energy, or fracture toughness, of the materials. For a more detailed discussion of fracture mechanics theory, see Kinloch and Young [4].

Glassy thermoplastic and thermoset materials meet the requirements for LEFM analysis. Indeed, LEFM techniques have been widely used in the study of amorphous, glassy thermoplastics [5–9] and thermosets [5, 10], especially brittle [11–18] and rubber toughened epoxies [19–21]. The environmental durability of these materials has been studied in the LEFM context as well [22, 23]. Primarily these studies have been concerned with Mode I, or cleavage loading. There have been relatively few investigations of mixed-mode loading [24, 25]. The other principal loading modes are in-plane shear (Mode II) and torsional, or anti-plane, shear (Mode III). Mode I testing has predominated since it is a common load condition (peel), and since, in general, materials

0022–2461/88 $03.00 + .12

TABLE I Materials

Material	Supplier	EEW*	M_N	M_W	M_W/M_N	Comment
D.E.N. 431	Dow chemical	172–179	400	500	1.25	Epoxy novolac resin
Epi-Rez 5048	Celanese Plastics and Specialities	145–165	400	400	1.00	Aliphatic triglycidyl ether resin
AP-5	Archem Corporation	–	140	–	–	1-[2-hydroxypropyl] -2-methylimidazole

appear to have the greatest fracture sensitivity to cleavage loading [26].

It should also be noted that, due to the viscoelastic nature of polymeric materials, fracture toughness is not a true material property since it is also a function of time (loading rate) and temperature. G_c also depends on sample thickness. The dependence on thickness is a result of the state of stress at the crack tip. In thick samples a condition of plane strain (triaxial stress) exists at the crack tip, while in thin samples plane stress (triaxial strain) occurs. Mode I toughness (G_{Ic}) will be greater for conditions of plane strain than for plane stress. Thus, for adhesively bonded samples, bond line thickness is an important parameter. Additionally for adhesive bonds, surface preparation techniques may influence joint toughness. Despite these limitations, fracture mechanics testing, as shown by the large body of LEFM studies, can lead to a fundamental understanding of crack propagation within structural polymeric materials.

In this investigation the Mode I fracture energy (or fracture toughness) (G_{Ic}) of three unfilled, imidazole-cured, epoxy novolac adhesives modified with various amounts of a reactive aliphatic epoxy, has been determined. Despite the considerable number of LEFM investigations of epoxy thermosets, few previous references to fracture mechanics studies of imidazole-cured materials were found. Epoxy/imidazole systems form high strength networks with excellent high temperature properties and good chemical and environmental resistance [27]. Such systems crosslink at both low (long time) and high temperatures [28]. The kinetics of the crosslinking reactions are complicated and not fully understood [29, 30], however. Additionally, aromatic/aliphatic epoxy mixtures have not been widely investigated by LEFM techniques. From the various Mode I testing geometries available [31–34], the tapered double cantilevered beam (TDCB) geometry was chosen for this work. This experimental approach, developed by Mostovoy and Ripling [35], is valid for bulk adhesive (cohesive fracture), as well as adhesive joint testing [36]. Here, bulk toughness was obtained and related to the morphology of the fracture surface observed by scanning electron microscopy. Also, previously determined [30] structural (crosslink density) and thermal characteristics of these formulations were correlated to the measured fracture toughness.

2. Materials

The materials used, suppliers, molecular weights and dispersities as determined by gel permeation chromatography, epoxy equivalent weight (EEW), and various comments regarding the materials are listed in Table I. Dow Epoxy Novolac 431 (D.E.N. 431) and Celanese Epi-Rez 5048, a reactive, aliphatic epoxy modifier, were used as received. The curing agent, [1-(2-hydroxypropyl)-2-methylimidazole] (AP-5) was distilled (145° C, 2 mm Hg) prior to use. The structures of these materials are given in Fig. 1.

3. Sample preparation

The three formulations shown in Table II were prepared for fracture mechanics testing. The formulations are referred to by a formulation number followed by, in parentheses, the weight per cent Epi-Rez 5048. This nomenclature is consistent with that used in previous work [30]. All formulations have a ratio of curing agent to total epoxide functionality of 0.113.

For each formulation, the indicated amounts of aromatic and aliphatic epoxy resins were mixed and degassed at 100° C for five to six hours, maintained under vacuum overnight, and then reheated to 100° C for four hours. This mixture was cooled and the

TABLE II Formulations

Formulation	D.E.N. 431 (g)	Epi-Rez 5048		Ap-5 (g)
		(g)	wt %*	
3(33)	120.0	60.0	33	16.9
4(43)	100.0	75.0	43	16.6
5(50)	90.0	90.0	50	17.2

*Weight per cent with respect to resin only.

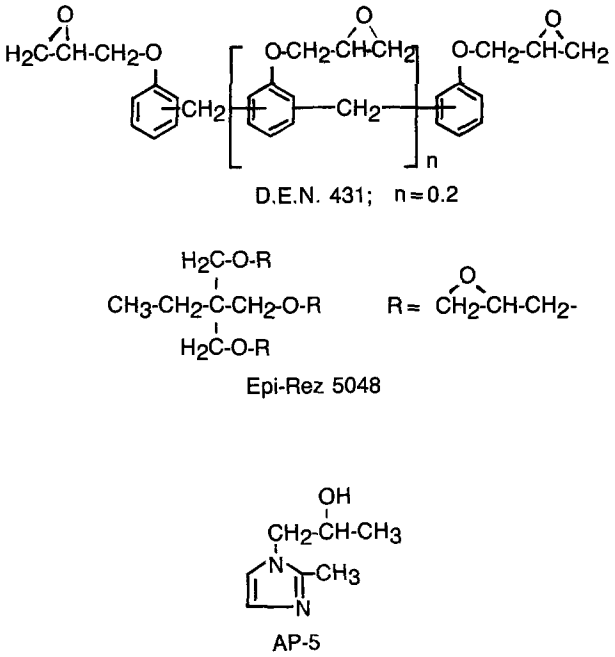

Figure 1 Structures.

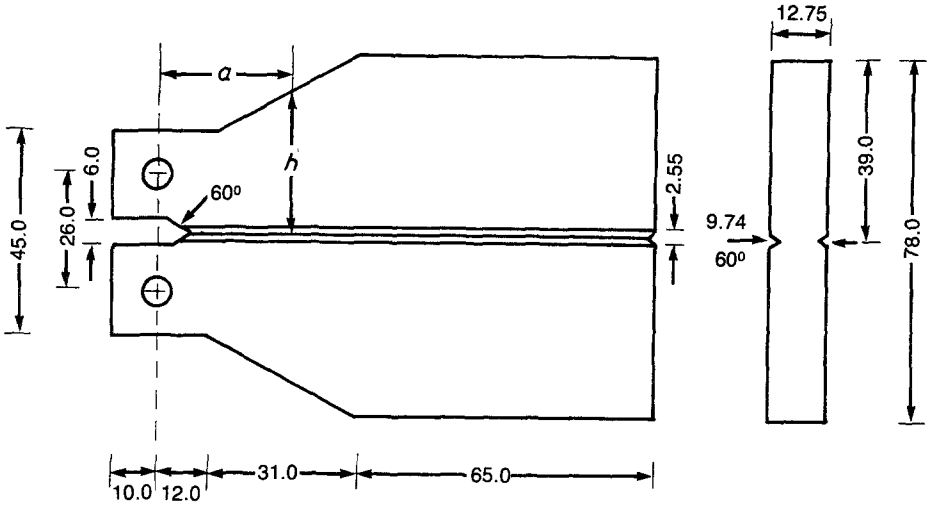

Figure 2 Dimensions in millimetres for the TDCB samples, and a typical sample.

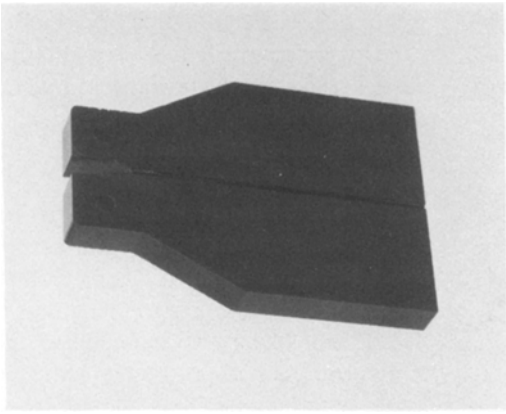

appropriate amount of curing agent was added under vacuum, after which the mixture was poured into a Frekote Lifft-coated, tapered double cantilevered beam (TDCB) mold. This aluminium mould consisted of two plates with 60° wedges which formed side grooves in the beam samples. These grooves acted as crack guides. The third piece, which was placed between the two face plates, was the beam template. The mould was supported in an upright position as the resin mixture was poured in, and while the mixture underwent a 24 hour room temperature gel. After 24 hours the mould was placed in a forced air oven at 150° C for 30 minutes, cooled to room temperature, and then the beam sample was de-moulded. Loading holes, 6.5 mm in diameter, were either drilled through, or moulded in the arms of the beams to accommodate Instron loading pins. A typical beam sample, along with its dimensions, is shown in Fig. 2. All samples were subjected to a standard post-cure cycle* one day prior to testing.

4. Fracture toughness testing

Compliance calibration, and toughness and flex modulus measurements were all performed at room temperature.

4.1. Compliance calibration

Compliance calibration was performed for each of the three formulations to be tested. A crack of known length, a, was sawn through the beam sample. The beam was then mounted, using 6.4 mm diameter pins through the loading holes described above, in an Instron Model 1125 Universal Testing Machine. An extensiometer was attached to the loading pins to measure displacement, and compliance (i.e. displacement as a function of load) was measured for this known crack length at a loading rate of 0.05 mm min^{-1}. This was repeated several times, each time sawing a new crack of increased length in the same beam. A plot of compliance against crack length was then constructed.

4.2. Toughness measurements

To carry out actual toughness measurements, beam samples, without the saw cut, were mounted in the Instron as described above and strained at a constant rate of 0.05 mm min^{-1}. As fracture occurred, load as a function of displacement was recorded on a strip chart recorder until the beam was fractured along its entire length. For most of the beams, crack arrest and re-initiation occurred several times during an experiment. For each crack initiation and arrest along a beam, the crack initiation, or critical load together with the arrest load (P_c and P_a, respectively) was obtained from the measured load against displacement curves. If the crack did not propagate

*Post-cure cycle: 25 min at 200° C; cool to room temperature; 75 min at 160° C; cold water quench to room temperature; 30 min at 135° C; cool to room temperature; 20 min at 135° C; cool to room temperature; 40 min at 160° C; cool to room temperature.

perpendicular to the applied load, that is, parallel to the moulded-in side grooves, the experiment was stopped and data from the "out-of-guide groove" portion of the crack was not used. Usually, when this occurred one of the beam arms would break off. Also, for the LEFM analysis to be valid, P_c and P_a must be obtained from "natural", sharp-tipped, cracks. For this reason, since the first crack of each beam initiates from the blunt, molded-in notch, data from the first crack of all the beams was not used.

4.3. Flexural modulus

The flexural modulus of each formulation, necessary for the toughness analysis detailed below, was obtained in accordance with ASTM D-790. Samples (76.2 × 25.4 × 3.8 mm) were cut from sheets prepared as described above for TDCB, except that the resin was poured between two glass plates. These flexural samples were then tested on an Instron (Model TTC) testing machine using a three-point bending fixture with a 51 mm support span, at a loading rate of 1.27 mm min^{-1}.

5. LEFM analysis

For a stressed, flawed or cracked body exhibiting bulk linear elastic behaviour, the general expression for the strain energy release rate is [4]

$$G_c = (P_c^2/2b_n)(dC/da) = G_{Ic} \text{ (Mode I)} \quad (1)$$

where P_c is the load at the instant of crack propagation, b_n is the sample thickness in the vicinity of the crack (in this case, the thickness at the moulded in side grooves), and C is the compliance. C is a function of the crack length a and dC/da must be determined either experimentally or analytically for any given sample geometry. For Mode I loading, Mostovoy and Ripling [35] designed a tapered double cantilevered beam (TDCB) sample for which dC/da is constant. For this specimen geometry, it follows from beam theory that

$$G_{Ic} = (4P_c^2/bb_nE)(3a^2/h^3 + 1/h) \quad (2)$$

where P_c, a, and b_n are defined as above, b is the bulk sample thickness, E is Young's modulus (in this case the flex modulus), and h is the beam height at crack length a (see Fig. 2). If the beam is contoured such that the second term in Equation 2 is approximately a constant, Equation 2 may be replaced by

$$G_{Ic} = 4P_c^2m/bb_nE \quad (3)$$

where m describes the beam contour. For a simple elastic beam of this configuration, compliance changes linearly with crack length, i.e., dC/da is constant, and G_{Ic} is only a function of the load at crack propagation. This sample configuration and analysis is applicable to bulk (cohesive) and adhesive joint testing, although the taper must be steeper for bulk samples [26]. For the TDCB samples in this work, $a/h \approx 1$, $m = 121.3\ m^{-1}$ (3.08 in^{-1}), and the taper was approximated by a straight line. The load applied to the TDCB samples was perpendicular to the moulded in side grooves so that the crack propagated along the side grooves.

Linearity of compliance with crack length for a TDCB sample of a given material must be confirmed for the LEFM analysis to be valid. It is possible for a material to exhibit bulk linear elastic behaviour, with dC/da equal to a constant, even when inelastic deformation occurs at the crack tip [4]. Thus, as long as plastic deformation is restricted to a small zone at the crack tip, this analysis may be applied. The compliance calibration described above involved measuring C at several known crack lengths, a, along a given beam and plotting C as a function of a. If a straight line is obtained, the overall behaviour of the sample material, regardless of what occurs at the crack tip, is linear. Thus dC/da is constant, and Equation 3 may be used to calculate G_{Ic}.

As well as determining the linearity of compliance with crack length, compliance calibration has also been used to calculate a "corrected" value for the beam contour parameter m, which is designated m' [26, 36]. Once dC/da has been obtained from the slope of the compliance calibration plot, Equations 1 and 3 are combined such that

$$\tfrac{1}{8}b_nE\,(dC/da) = m' \quad (4)$$

and m' is used in place of m in Equation 3. This is done to correct for deviations from assumptions of beam theory, which occur for beams with steep tapers, such as those used in this work. There is, however another factor which may be included in the m' correction. Since compliance can be associated with an effective crack length rather than the actual crack length [37], any plastic deformation at the crack tip is accounted for in the (dC/da) term, along with beam theory corrections. Thus, localized plastic contributions to the behaviour of bulk linear elastic materials are included in m'. In this work, rather than calculating m' and comparing toughness values from the two versions of Equation 3, values of fracture toughness obtained from Equations 1 and 3 (uncorrected) will be compared directly.

6. Results and discussion

6.1. Compliance calibration

Compliance for formulations 3(33), 4(43), and 5(50), increased linearly with increasing crack length (Table III). A typical C against a plot is shown in Fig. 3. Thus, the LEFM analysis was judged to be valid for these formulations. From the slopes of the C against a plots, dC/da for formulations 3(33), 4(43), and 5(50) were found to be $5.26 \times 10^{-5}\ N^{-1}$, $5.56 \times 10^{-5}\ N^{-1}$, and $7.04 \times 10^{-5}\ N^{-1}$, respectively.

6.2. Fracture toughness

A load–displacement curve representative of the fracture toughness determinations for all three epoxy formulations is shown in Fig. 4. This "saw-tooth" behaviour is defined as "stick–slip", or brittle, unstable fracture [10]. In this type of fracture, the sample deforms elastically until the critical load, P_c, is reached. The crack then propagates along the beam until the strain energy decreases to an extent sufficient to allow crack arrest. The mechanisms responsible for crack arrest are discussed below. The load at arrest (P_a) is

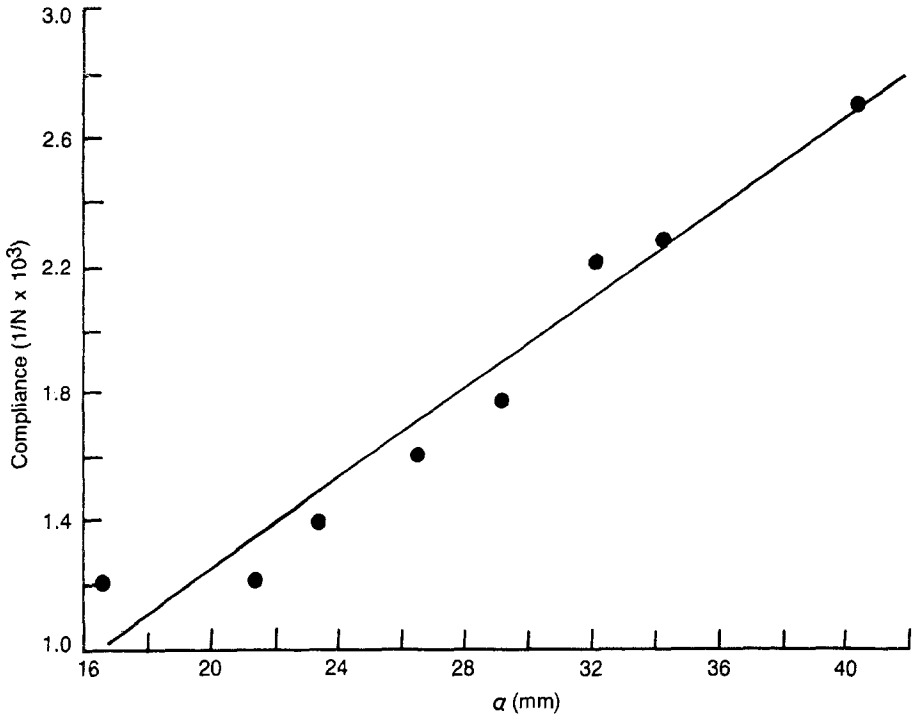

Figure 3 Compliance calibration for formulation 5(50).

indicated in Fig. 4. Crack propagation, arrest, and re-initiation occurred two to five times for a given beam sample, a maximum of three valid P_c values were obtained for these beams. For each formulation a number of beams were tested; the critical loads are tabulated in Table IV.

Fracture toughness, as calculated from both Equation 3 and Equation 1, is given in Table V. As shown in Fig. 5, as the amount of aliphatic epoxy (Epi-Rez 5048) in the formulation increased, the fracture toughness, whether calculated from Equation 3 or Equation 1, increased. For all three formulations, G_{Ic} (Equation 1) was greater than G_{Ic} (Equation 3). Additionally, as the amount of aliphatic epoxy increased, the difference between G_{Ic} (Equation 1) and G_{Ic} (Equation 3) increased.

That G_{Ic} (Equation 3) is different from G_{Ic} (Equation 1) for each of the three epoxy formulations, 3(33), 4(43), and 5(50), and that the magnitude of the difference is a function of formulation (Table V), can be explained by considering the extent to which the two equations account for plastic deformation during fracture. As noted in the LEFM analysis (Section 5), the parameter m in Equation 3 should be replaced by m'. This parameter is related to an effective crack length, and includes any plastic zone at the crack tip. In Equation 1, plastic contributions to fracture toughness are contained in the compliance term, dC/da. Thus, if the m to m' correction is not made, the difference between G_{Ic} (Equation 1) and G_{Ic} (Equation 3) may be interpreted as a qualitative indication of the amount of deformation during fracture. (The difference in G_{Ic} values arising from beam theory corrections will be assumed to be constant for these three formulations.) Consequently, for extremely brittle materials the toughness calculated using the two equations should

TABLE III Compliance calibration

Formulation 3(33)		Formulation 4(43)*		Formulation 5(50)	
a (mm)	C (mm N^{-1} × 10^3)	a (mm)	C (mm N^{-1} × 10^3)	a (mm)	C (mm N^{-1} × 10^3)
14.65	1.32	12.27	1.71	16.60	1.21
16.10	1.63	12.39	0.825	21.36	1.22
16.96	1.72	14.88	0.860	23.41	1.40
18.46	1.12	16.56	1.60	26.40	1.61
21.10	1.35	17.85	1.38	29.11	1.78
23.34	1.48	20.74	1.34	32.15	2.22
25.94	1.89	22.11	1.40	34.28	2.29
28.68	2.22	24.76	1.75	40.50	2.72
33.85	2.37	26.68	1.65		
37.11	2.55	31.69	2.29		
40.52	2.58	34.71	1.82		
		35.12	2.26		
		39.60	3.23		
		40.10	2.49		
Slope (dC/da) = 5.26 × 10^{-5} N^{-1}		Slope (dC/da) = 5.56 × 10^{-5} N^{-1}		Slope (dC/da) = 7.04 × 10^{-5} N^{-1}	
Correlation = 0.902		Correlation = 0.848		Correlation = 0.977	

*Results from two compliance tests combined.

TABLE IV Critical load, P_c

Formulation 3(33)			Formulation 4(43)			Formulation 5(50)		
Beam number	Crack number	P_c (kN)	Beam number	Crack number	P_c (kN)	Beam number	Crack number	P_c (kN)
1	1	0.334	1	1	0.462	1	1	0.512
2	1	0.338	2	1	0.436	2	1	0.547
3	1	0.320		2	0.480	3	1	0.476
	2	0.329	3	1	0.454	4	1	0.387
	3	0.338	4	1	0.543		2	0.409
4	1	0.338	5	1	0.489	5	1	0.556
	2	0.351	6	1	0.436			
5	1	0.311		2	0.360			
	2	0.334	7	1	0.356			
			8	1	0.396			

P_c (avg) = 0.332 ± 0.01 kN P_c (avg) = 0.441 ± 0.06 kN P_c (avg) = 0.481 ± 0.07 kN

be nearly identical. Alternatively, where G_{Ic} (Equation 1) is greater than G_{Ic} (Equation 3), as it is for the formulations investigated in this work, some degree of plastic deformation has occurred during fracture. Also, as toughness increased, the difference in the G_{Ic} values for the two equations increased. This suggests that increasing toughness is due to an increased ability to absorb, or dissipate, energy by plastic deformation. As will be discussed in the next section, scanning electron microscopy confirmed that there was greater fracture surface roughness (deformation) for the samples with higher G_{Ic} values.

At some point, i.e., at some extent of plasticity, the linear elastic treatment is no longer valid. (Even at this point, dC/da might still be constant over a given range of crack lengths.) In this work, since G_{Ic} is used as a qualitative indication of toughness and plasticity, no attempt was made to determine the limit of LEFM applicability.

6.3. Fractography investigation of fracture and arrest mechanisms

Examination of the micrographs in Figs 6–8 shows that the fracture surfaces of formulations 3(33)–5(50) do, in fact, exhibit increasing evidence of plastic deformation as G_{Ic} increases. Fracture surfaces of each of the formulations have "fingernail" marks crossing the width of the sample, perpendicular to the crack direction (Figs 6a–8a; the crack direction is from left to right in the micrographs). The markings correspond to the crack arrest position [33, 38–40]. These arrest marks, which are evidence of deformation, become more prominent as the sample toughness increases. Micrographs of regions removed from the arrest markings (Figs 6b–8b) also demonstrate that plasticity increased as the weight per cent aliphatic epoxy in the formulations increased. The features in Fig. 6b are long, regular, sharply edged lines running parallel to the crack direction. In Figs 7 (formulation 4(43)) and 8 (formulation 5(50)) these striations become less regular so that the surface becomes rougher and more textured. No evidence of crazing was observed for any of the fracture surfaces examined.

The series of events which occur in stick–slip fracture have been described by Phillips *et al.* [41], Kinloch and Williams [42], Yamini and Young [38], and Kinloch and Young [10]. After crack arrest, as loading continues, a plastic zone develops at the crack tip. Local small-scale yielding forms a deformation zone and causes crack tip blunting. This blunt-tipped crack grows slowly until sufficient strain energy is stored, through continued loading, to force the crack to jump rapidly ("slip") through undeformed material. This "fast" crack has a sharp tip as there is insufficient time for any appreciable deformation to occur. Since the crack propagates rapidly, it "outruns" the stress field (the loading) and eventually arrests once again ("sticks") at reduced load, P_a. Thus, the crack velocity does not depend on the loading rate.

The slow growth region described above appears

TABLE V Fracture toughness, G_{Ic}

Formulation	G_{Ic} (J m^{-2})	
	Equation 3*	Equation 1
3(33)	163	305
4(43)	283	569
5(50)	330	857

*Flex modulus: Formulation 3(33); E = 1750 ± 32 kN in^{-2}
Formulation 4(43); E = 1770 ± 39 kN in^{-2}
Formulation 5(50); E = 1810 ± 31 kN in^{-2}

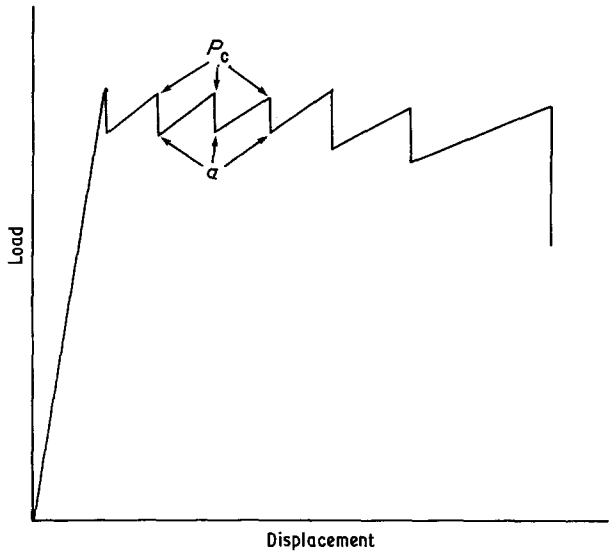

Figure 4 Typical load–displacement curve for brittle, unstable fracture.

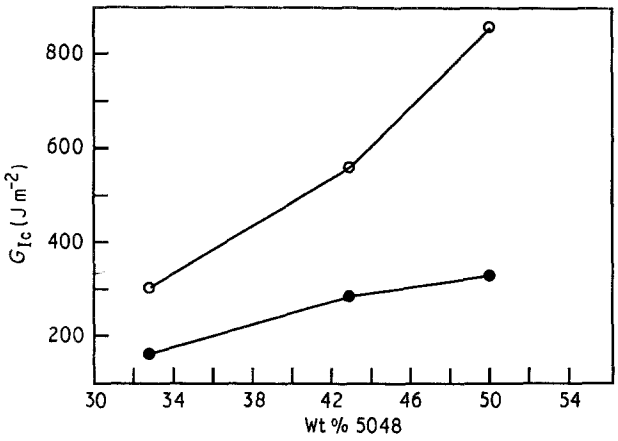

Figure 5 Fracture toughness, Equations 3 (●) and 1 (○), as a function of formulation.

to be related to a Dugdale plastic zone [4, 10]. In the Dugdale line model, the plastic zone extends the effective crack length by the length of the zone. Therefore, it is the slow-growth, re-initiation process that produces the "arrest" features visible on the micrographs. The width of the fingernail mark indicates the size of the plastic zone. For epoxies, Yamini and Young [38] report arrest mark widths of 6 to 160 μm, depending on loading rate and test temperature. The widths of the fingernail marks in Figs 6a–8a are $\sim 21\,\mu$m for formulation 3(33) and ~ 40–$50\,\mu$m for formulations 4(43) and 5(50), indicating an increase in the size of the plastic zone as the amount of aliphatic epoxy in the formulation was increased.

Moloney and Kausch [43] were able to directly observe fracture in an anhydride-cured epoxy. They noted that the region of slow crack growth was comprised of a blunt crack tip surrounded by a highly deformed zone ($\sim 50\,\mu$m) which included numerous microcracks. The formation of these microcracks, and the yielding that occurs around them, are energy absorbing processes which are responsible for increases in toughness. It has been suggested [43] that the subsequent propagation of a fast crack through this zone of microcracks causes the striations observed in brittle fracture surfaces (see Figs 6b–8b). The microcracks, formed at slightly different heights with respect to the main crack, propagate through the sample at these different levels creating the surface features. Therefore, as toughness increases, plasticity, deformation, microcracking, and fracture surface roughness increase. As noted at the beginning of this section, an increase in roughness was observed in the order of formulation 3(33) < 4(43) < 5(50) (Figs 6b–8b).

6.4. Fracture toughness and network properties

The epoxy resin/curing agent ratio and post-cure temperature have been shown to influence the fracture energy, or toughness of other crosslinked epoxy systems [15, 36]. Presumably, these experimental

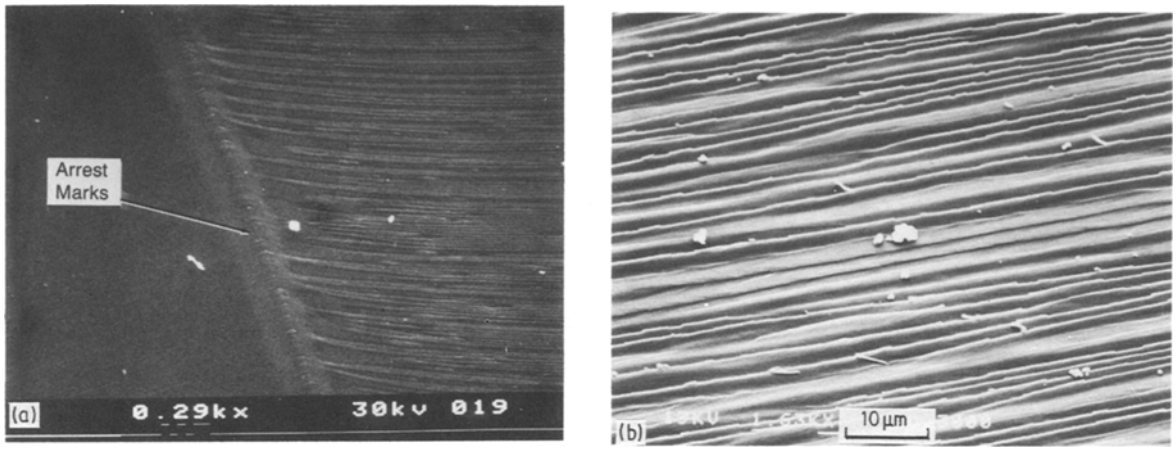

Figure 6 Fracture surfaces for formulation 3(33); (a) arrest mark, 188 ×, and (b) striations, 1059 ×.

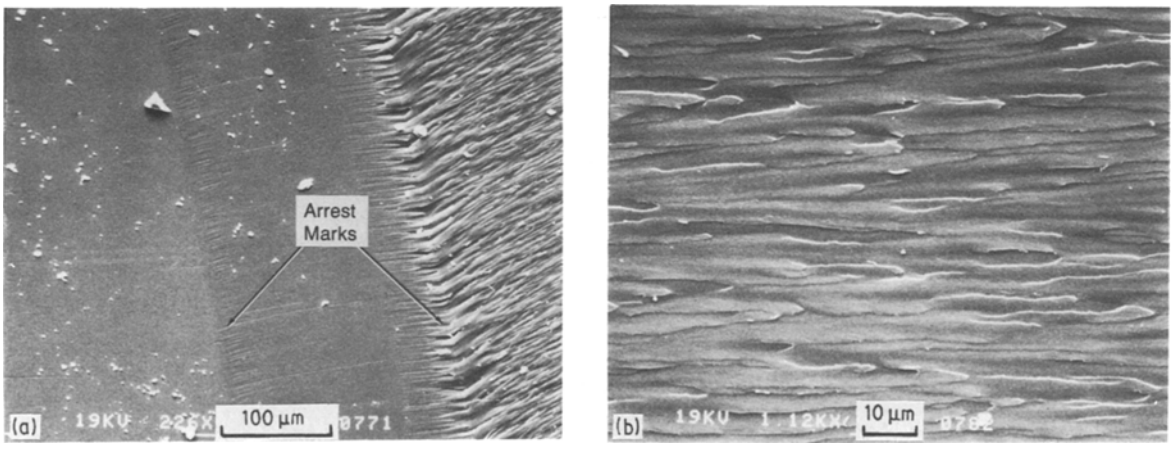

Figure 7 Fracture surfaces for formulation 4(43); (a) arrest mark, 147 ×, and (b) striations, 728 ×.

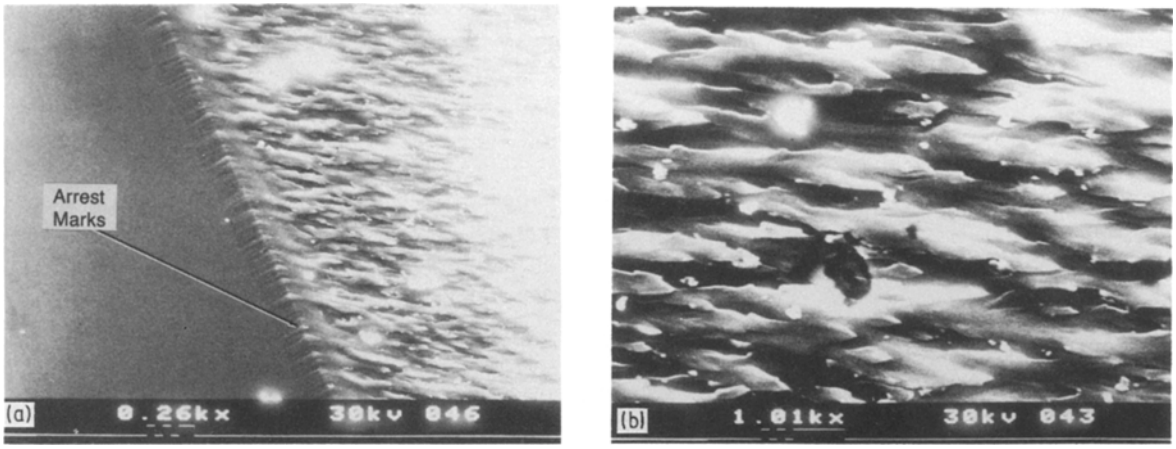

Figure 8 Fracture surfaces for formulation 5(50); (a) arrest mark, 169 ×, and (b) striations, 656 ×.

parameters affect, at least to some degree, the crosslink density of the network. Indeed, for a crosslinked poly(methyl methacrylate) system, the fracture toughness was shown to decrease with increasing crosslink density [10]. Thus, network structure is expected to influence the fracture toughness of the epoxy networks in this work, even though network structure was altered by changing the aromatic/aliphatic epoxy ratio rather than the amount of curing agent, reaction time, or post-cure temperatures. Network crosslink density and the thermal characteristics of the networks used in the present study were analysed previously [30]. The relationships of these characteristics with the fracture behaviour observed here were investigated.

As shown in Fig. 9, fracture toughness of formulations 3(33), 4(43), and 5(50) increased as the crosslink density, $1/M_c$, decreased. (M_c is defined as the molecular weight between crosslinks.) This was expected since chain mobility should increase with decreasing crosslink density [30]. Decreasing the number of network tie-points allows a greater amount of plastic deformation to occur before chain scission, and, therefore, bulk fracture, commences. Since it was found [30] that there is a direct relationship between crosslink density and glass transition temperature, T_g, a relationship between G_{Ic} and T_g was also expected. Indeed, Fig. 10 shows that, as with crosslink density, fracture toughness increased with decreasing T_g.

It has been demonstrated above that the fracture toughness of the three unfilled, glassy thermoset networks is a function of their ability to absorb (or dissipate) energy in plastic deformation. The energy absorbing mechanism in the glassy state which is associated with segmental and/or side group motion along polymer chains and, therefore, small scale

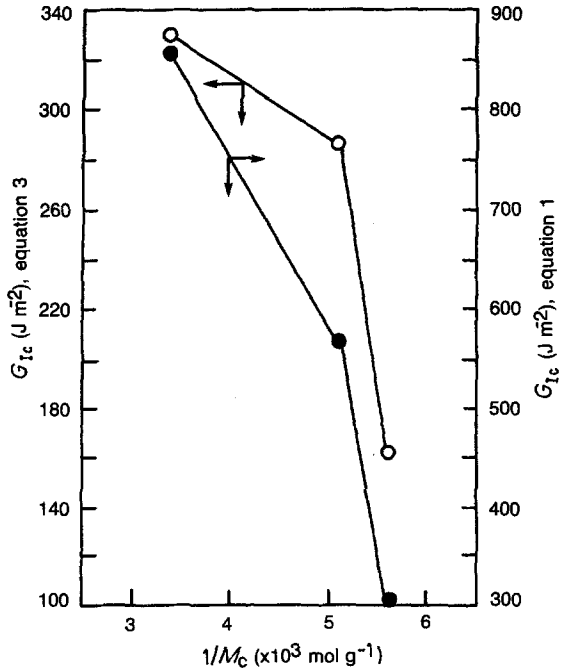

Figure 9 Fracture toughness (Equations 3 (LHS) and 1 (RHS)) as a function of crosslink density.

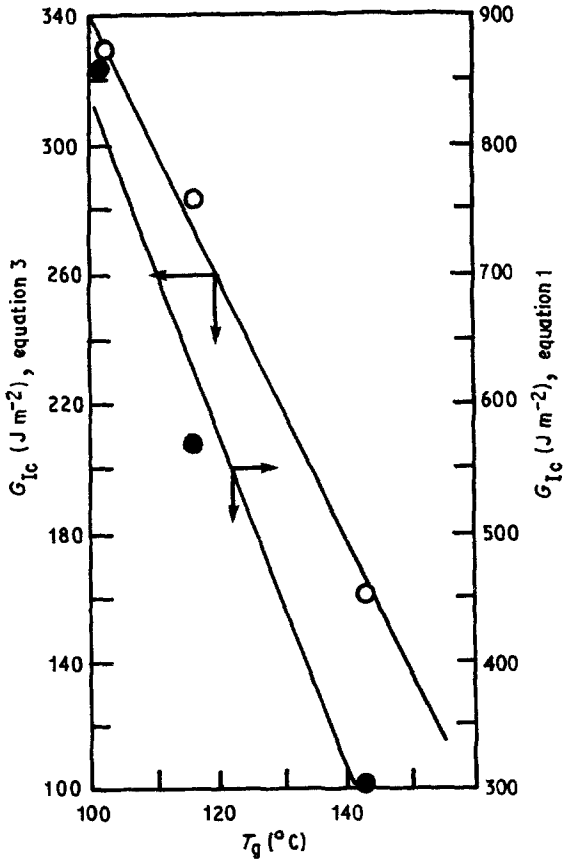

Figure 10 Fracture toughness (Equations 3 and 1) as a function of glass transition temperature.

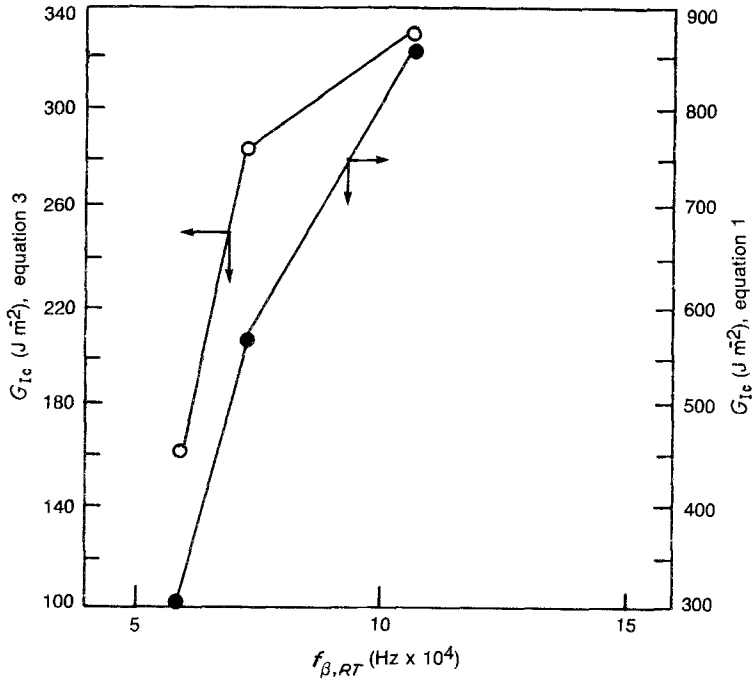

Figure 11 Fracture toughness (Equations 3 and 1) as a function of room temperature frequency of the β-transition.

deformation, is the β-transition [44, 45]. This transition is the highest temperature glassy state (sub-T_g) relaxation. Boyer [46] proposed that toughness should increase with an increase in the room temperature frequency ($f_{\beta,RT}$) of the β-transition. Values of $f_{\beta,RT}$ for formulations 3(33)–5(50) were calculated previously [30]. As can be seen in Fig. 11, fracture toughness was found to be a function of $f_{\beta,RT}$, with G_{Ic} increasing as $f_{\beta,RT}$ increases. Thus, it is likely that glassy state relaxations also play a role in determining fracture toughness.

7. Concluding remarks

The toughness, or fracture energy, of three unfilled epoxy adhesive formulations was determined using a linear elastic fracture mechanics analysis. G_{Ic} increased as the amount of aliphatic epoxy modifier increased. Examination of fracture surface morphologies of these materials demonstrated that toughness is a function of the ability of the material to undergo plastic deformation. Therefore, toughness was expected to be a function of network structure. Indeed, toughness increased as crosslink density and T_g decreased. The glassy state relaxation, T_β, also correlated with toughness via its relationship to energy dissipation during crack propagation.

Knowledge of the correlations between mechanical properties and chemical and structural variables will ultimately enable the optimization of specific properties, such as adhesive strength and durability, high temperature response, and fracture toughness, for structural adhesives, enabling adhesive joints to be used in a wider variety of applications.

Acknowledgements

I would like to thank Dr W. C. Meluch, Mr E. M. Hagerman (Polymers Department, General Motors Research Laboratories), and Dr S. Mostovoy (Illinois Institute of Technology) for helpful discussions.

References

1. A. A. GRIFFITH, *Phil. Trans. R. Soc.* **A221** (1920) 163.
2. E. OROWAN, *Rep. Prog. Phys.* **12** (1948) 185.
3. G. R. IRWIN, *J. Appl. Mech. Trans. ASME* **24** (1957) 361.
4. A. J. KINLOCH and R. J. YOUNG, "Fracture Behavior of Polymers" (Applied Science Publishers, New York, 1983) Chapter 3.
5. G. PRITCHARD and G. V. RHOADES, *Mater. Sci. Eng.* **26** (1976) 1, and references therein.
6. L. J. BROUTMAN and F. J. McGARRY, *J. Appl. Polym. Sci.* **9** (1965) 609.
7. R. P. KAMBOUR, A. S. HOLIK and S. MILLER, *J. Polym. Sci., Polym. Phys. Edn* **16** (1978) 91.
8. G. P. MARSHALL, L. E. CULVER and J. G. WILLIAMS, *Proc. R. Soc. Lond.* **A319** (1970) 165.
9. A. J. KINLOCH and R. J. YOUNG, "Fracture Behavior of Polymers" (Applied Science Publishers, New York, 1983) Chapter 7.
10. *Idem, ibid.* Chapter 8.
11. W. D. BASCOM, R. L. COTTINGTON, R. L. JONES and P. PEYSER, *J. Appl. Polym. Sci.* **19** (1975) 2545.
12. R. A. GLEDHILL, A. J. KINLOCH, S. YAMINI and R. J. YOUNG, *Polymer* **19** (1978) 574.
13. R. Y. TING and R. L. COTTINGTON, *Adh. Age* **24** (1981) 35.
14. R. A. GLEDHILL and A. J. KINLOCH, *Polym. Eng. Sci.* **19** (1979) 82.
15. R. GRIFFITHS and D. G. HOLLOWAY, *J. Mater. Sci.* **5** (1970) 302.
16. J. MIJOVIĆ, *J. Appl. Polym. Sci.* **25** (1980) 1179.
17. S. MOSTOVOY and E. J. RIPLING, *ibid.* **15** (1971) 661.
18. J. MIJOVIĆ, *ibid.* **27** (1982) 2919.
19. D. L. HUNSTON, J. L. BITNER, J. L. RUSHFORD, J. OROSHNIK and W. S. ROSE, *J. Elast. Plast.* **12** (1980) 133.
20. A. J. KINLOCH, S. J. SHAW and D. L. HUNSTON, *Polymer* **24** (1983) 1355.
21. D. L. HUNSTON and W. D. BASCOM, in "Rubber-Modified Thermoset Resins", edited by C. K. Riew and J. K. Gillham (American Chemical Society, Washington, DC, 1984) p. 101.
22. S. MOSTOVOY and E. J. RIPLING, *J. Appl. Polym. Sci.* **15** (1971) 611.
23. S. YAMINI and R. J. YOUNG, *Polymer* **18** (1977) 1075.
24. E. J. RIPLING, J. S. SANTNER and P. B. CROSLEY, *J. Mater. Sci.* **18** (1983) 2274.

25. G. P. ANDERSON, K. L. DEVRIES and M. L. WILLIAMS, *Int. J. Frac.* **10(5)** (1974) 565.
26. E. J. RIPLING, S. MOSTOVOY and H. T. CORTEN, *J. Adhesion* **3** (1971) 107.
27. A. F. FARKAS and P. F. STROM, *J. Appl. Polym. Sci.* **12** (1968) 159.
28. SHELL CHEMICAL COMPANY, Epon® Resin Structural Reference Manual.
29. F. RICCIARDI, W. A. ROMANCHICK, M. M. JOULLIE, *J. Polym. Sci., Polym. Chem. Edn* **21** (1983) 1475.
30. J. A. SCHROEDER, P. A. MADSEN and R. T. FOISTER, *Polymer* **28** (1987) 929.
31. J. M. SCOTT, G. M. WELLS and D. C. PHILLIPS, *J. Mater. Sci.* **15** (1980) 1436.
32. R. Y. TING and R. L. COTTINGTON, *J. Appl. Polym. Sci.* **25** (1980) 1815.
33. A. J. KINLOCH, S. J. SHAW, D. A. TODD and D. L. HUNSTON, *Polymer* **24** (1983) 1341.
34. A. C. MOLONEY, H. H. KAUSCH and H. R. STIEGER, *J. Mater. Sci. Lett.* **3** (1984) 776.
35. S. MOSTOVOY and E. J. RIPLING, *J. Appl. Polym. Sci.* **10** (1966) 1351.
36. S. MOSTOVOY, E. J. RIPLING and C. F. BERSCH, *J. Adhesion* **3** (1971) 125.
37. S. MOSTOVOY, P. B. CROSLEY and E. J. RIPLING, *J. Mater. Sci.* **2** (1967) 661.
38. S. YAMINI and R. J. YOUNG, *ibid.* **15** (1980) 1823.
39. R. L. PATRICK, W. G. GEHMAN, L. DUNBAR and J. A. BROWN, *J. Adhesion* **3** (1971) 165.
40. B. W. CHERRY and K. W. THOMSON, *J. Mater. Sci.* **16** (1981) 1925.
41. D. C. PHILLIPS, J. M. SCOTT and M. JONES, *ibid.* **13** (1978) 311.
42. A. J. KINLOCH and J. G. WILLIAMS, *ibid.* **15** (1980) 987.
43. A. C. MOLONEY and H. H. KAUSCH, *J. Mater. Sci. Lett.* **4** (1985) 289.
44. D. C. TIMM, A. J. AYORINDE and R. F. FORAL, *Brit. Polym. J.* **17(2)**, (1985) 227.
45. E. SACHER, *J. Appl. Polym. Sci.* **19** (1975) 1421.
46. R. F. BOYER, *Polymer.* **17** (1976) 996.

Received 3 April
and accepted 22 October 1987